Imitation Learning of Humanoid Locomotion Using the Direction of the Landing Foot

WOOSUNG YANG and NAK YOUNG CHONG *

Center for Cognitive Robotics Research, Korea Institute of Science and Technology, P.O.BOX 131, Cheongryang, Seoul 130-650, Korea, (e-mail: wsyang@kist.re.kr)

School of Information Science, Japan Advanced Institute of Science and Technology, 1-1 Asahidai, Nomi, Ishikawa 923-1292, Japan, (e-mail: nakyoung@jaist.ac.jp)

Abstract. Since it is quite difficult to create motions for humanoid robots having fairly large numbers of degrees of freedom, it would be very convenient indeed if robots could observe and imitate what they want to create. Toward this end, this paper discusses how humanoid robots learn through imitation considering that demonstrator and imitator robots may have different kinematics and dynamics. As part of a wider interest in humanoid motion generation in general, this work mainly investigates how imitator robots adapt a reference locomotion gait captured from a demonstrator robot. Specifically, the self-adjusting adaptor is proposed, where the perceived locomotion pattern is modified to keep the direction of lower leg contacting the ground identical between the demonstrator and the imitator, and to sustain the dynamic stability by controlling the position of the center of mass. The validity of the proposed scheme is verified through simulations on OpenHRP and real experiments.

Index Terms *Humanoid robot, Biped locomotion, Imitation learning, Self-adjusting adaptor, ZMP*

I. INTRODUCTION

Stable and robust dynamic locomotion has been gaining increasing attention in the humanoid robot community, where considerable efforts have been devoted to how to deal with the highly nonlinear nature of robot dynamics and disturbances in uncertain environments. These efforts include such approaches as the zero moment point criterion [1-2], the linear inverted pendulum model [3], virtual model control [4], and biologically inspired approaches [5]. Even though certain methods do not depend heavily on the reference motion patterns, many existing methods employ some form of pattern generation and tracking control. This requires a fairly accurate robot model to compute dynamically admissible patterns. Since humanoid robots have a large

number of degrees of freedom (D.O.F.), efficient pattern generation still remains challenging. Thus, from a practical viewpoint, learning by imitation may be considered as another alternative for enhancing pattern generation competence.

Imitation learning has been widely studied in different areas [6-8]. Dasgupta and Nakamura proposed a method that makes motion capture data appropriately transferable to humanoid locomotion [9]. Regarding this problem, many researchers studied efficient imitation models to obtain reliable motion data in noisy stochastic environments [10-14]. Especially, Inamura *et al.* devised the mimesis model based on HMM which can imitate the motion of others and abstract the time-series motion patterns as symbol representation [10]. Samejima *et al.* suggested the framework MOSAIC, where plural dynamics and inverse dynamics are implemented to predict and control motions [13-14]. From the viewpoint of dynamics computation of kinematic chains, Nakamura and Ghodoussi [15] proposed an efficient scheme employing the Jacobian matrix of the unactuated joint angles with regard to the actuated ones. Nakamura and Yamane later extended this algorithm to develop an online motion generator [16], [17]. Their pioneering works solved dynamically challenging problems, but there still exist many practical issues resulting from actuator limitations of the imitator robot, uncertain nonlinearity of the contact and collision model, and the requirement for a large number and high accuracy motion capture data.

This paper addresses how to efficiently reduce uncertainties sufficient to raise doubts about existing methods, relying on the goal-directed imitation that leads to the fulfillment of the behavior's goal. In most cases, the captured motion data may not be straightforwardly used due to the kinematic and dynamic dissimilarities between the demonstrator and the imitator [18]. For this, we proposed the self-adjusting adaptor (SAA) to promote the imitator's ability to deal with internal structural constraints as well as external disturbances [19]. The SAA remains effective even when the robots closely interact with the environment. As part of behavior generation, this work mainly investigates the SAA-based imitation of locomotion that requires a finely tuned coordination of body segments as well as a stable interaction between the foot and the ground. Specifically, to inspect the significance of body dynamics, imitation is investigated for humanoid robots having different sizes and shapes. The validity of the proposed method is verified by simulations using the open architecture humanoid robotics platform, OpenHRP [20], and real experiments. For simplicity, we assume that 1) there are similarities in kinematic configurations

between the demonstrator and the imitator, 2) the COM position is located at the hip joint and will remain almost unchanged, whereby we can estimate the direction of the landing foot (or lower leg), because the demonstrator's COM position is difficult to be captured, 3) there is no foot rotation (or spinning) about an axis normal to the ground, and 4) when the stride foot lands down on the ground, it makes a complete surface contact with the ground. The foot contact is modeled as a point contact at the ankle joint. Hence, there is no slip between the stance foot and the ground.

Our contributions can be summarized in the following points. 1) For the motion capture data, only the Cartesian trajectories of the estimated center of mass (COM) and the distal end of the kinematic chain interacting with the environment (in this work, the ankle joint) are needed. Here, given the COM and ankle joint trajectories, the desired angle data of individual joints can be obtained by solving the inverse kinematics problem. Thus it is possible to generate each joint data of the imitator regardless of the difference in the D.O.F. between the demonstrator and the imitator. 2) Moreover, since the direction of landing of the lower leg of the imitator is kept identical with that of the demonstrator, the imitator locomotion becomes dynamically stable without requiring an additional balance controller if the demonstrator dynamics is known.

II. GOAL-DIRECTED IMITATION LEARNING

A. Goal-directed imitation between dissimilar bodies

When humans learn a specific skill from other humans, they are likely to observe and imitate the motion of the hand that directly interacts with the environment or object [21-23]. Our approach is inspired by this idea that enables the imitator to perform the most appropriate motion for attaining the goal of the behavior. Now, our concerns are the trajectories of the end-effector for producing the same interaction effect, and the COM for sustaining stability of bipedal locomotion. Note that, in contrast to prevailing approaches in imitation, we do not capture movements of all joints.

The difficulties of learning by imitation lie in how to deal with the dissimilar kinematics and dynamics of the demonstrator and the imitator. Our main idea is that the behaviors of the demonstrator and the imitator should bring the same effect to their environment [18-19]. To ensure that both robots satisfy this condition, the direction of the reaction force at the point of

action should be coincident between them. For instance, when learning tennis from a demonstrator having different link lengths, the imitator somehow needs to properly place the racket face vertically against the ball (See Fig. 1). In the figure, Cases 1 and 2 show that the intended goal might not be achieved if the imitator just copies the trajectories of joint angles or the end-effector of the demonstrator. In contrast, Case 3 illustrates that the imitator modifies the perceived trajectories to exert the same effect (some amount of force along the same direction) to the environment (the ball) as the demonstrator performs.

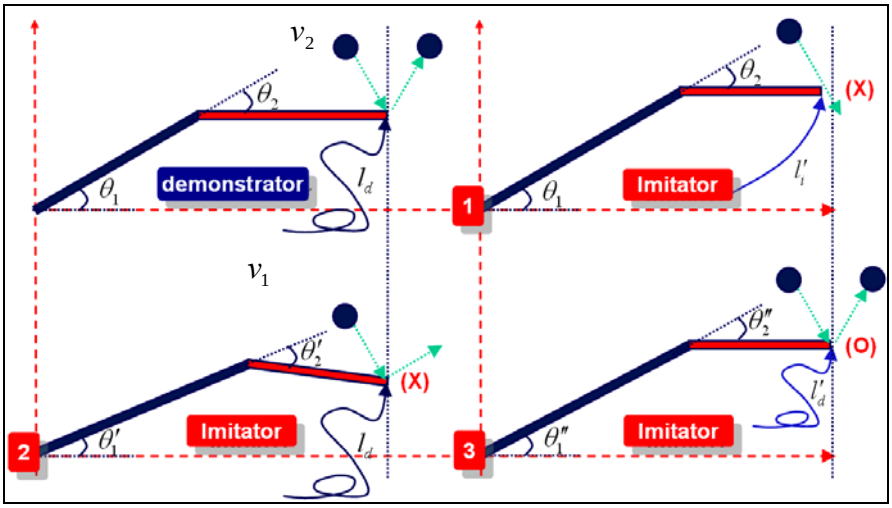

Fig. 1 Examples of imitation

B. Goal-directed imitation of biped locomotion

The imitator's prime concern should be the motion of the points of interest that interacts with the environment. Specifically, for the bipedal locomotion, the trajectories of the COM and the ankle joint are captured and these data are adapted to the kinematic structure of the imitator. Thus, in this paper, we propose that the landing direction needs to be kept identical between the demonstrator and the imitator, leading to a new approach to maintaining dynamic stability of the imitator as efficiently as possible exploiting the inverted pendulum approximation.

It is well known that the resultant moment of all external forces acting on a rigid body about a fixed point O is equal to the time derivatives of the angular momentum of the body about the same point given by

$$\sum M_O = \dot{H}_O, \tag{1}$$

where M_O and H_O are the moment (or torque) and the angular momentum about the point O, respectively. When a rigid body is rotating with angular velocity w about a fixed axis passing through the point O, the linear momentum, L, and the angular momentum, H_G, about the COM, G, are given by

$$\begin{aligned} H_G &= I_G w, \\ L &= m v_G, \end{aligned} \tag{2}$$

where I_G is the moment of inertia about the COM, m is the mass of the body, and v_G is the velocity of the COM. The angular momentum of the body can be written at the point O as

$$H_O = H_G + r_G \times L, \tag{3}$$

where r_G is the position vector from O to the COM of the body. Substituting Eq. (3) into Eq. (1) gives

$$\sum (r_i \times F_i) + r_G \times mg = \dot{H}_G + r_G \times \dot{L}, \tag{4}$$

where r_i is the position vector from O to the point at which the external force F_i is applied, and g is the gravitational acceleration. Eq. (4) can be rewritten as

$$\sum (r_i \times F_i) + r_G \times mg = \dot{H}_G + r_G \times m\dot{v}_G \tag{5}$$

If the angular momentum of the body is conserved, Eq. (5) becomes

$$\sum (r_i \times F_i) + r_G \times mg = r_G \times m\dot{v}_G \tag{6}$$

This equation means that the total moment about the COM is zero and the body has a constant angular velocity.

During stable biped locomotion as illustrated in Fig. 2, the angular momentum will be conserved despite the interaction of the feet with the ground. Thus, no external moment will be generated on the robot body.

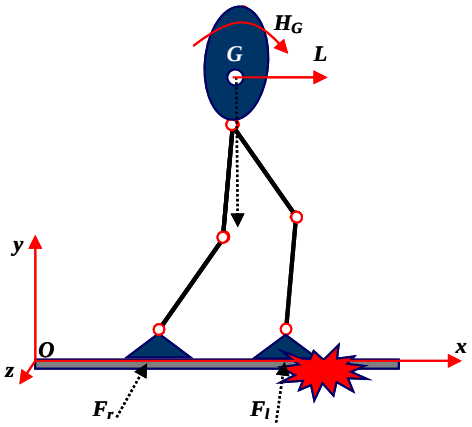

Fig. 2 Free body diagram of bipedal walking robot in a sagittal plane. F_r and F_l are reaction forces acted at the right foot and the left foot.

Referring to Fig. 2, Eq. (6) can be written as

$$r_l \times F_l + r_r \times F_r + r_G \times mg = r_G \times m\dot{v}_G, \tag{7}$$

This equation is equivalent to the eccentric impact model of two bodies constrained to rotate about a fixed axis at O, assuming that the stance foot is the axis of rotation. In Fig. 1, we assumed that the ball is stationary while the two-link arm rotates about a fixed axis. Thus, the model of Fig. 1 becomes identical to that of Fig. 2 as shown in Fig. 3 (a) and (b).

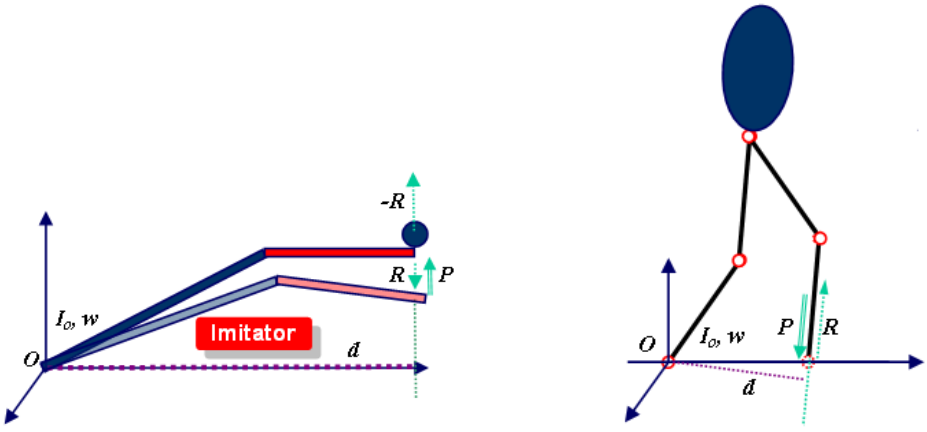

(a) (b)

Fig. 3 (a) the arm rotates and the racket face collides with the ball (b) the stride foot collides with the ground

During the collision, if the ground is presumably not rigid, Eq. (7) can be rewritten as

$$OR \times \int R dt + r_G \times m(g - \dot{v}_G) = 0, \tag{8}$$

where *OR* is the position vector from the origin of the axis to the reactive impulse force *R* after the impact, and *P* is the impulse force exerted on the ground during the deformation. Here the demonstrator locomotion can be considered as satisfying Eq. (8) and *m* is assumed to be known, while the variables *R* and *OR* should be determined to satisfy the stability requirement of the imitator. If the impulse force *R* of the demonstrator is identical with that of the imitator, we can determine the one of the imitator. However, in fact, the imitator may not maintain the stability condition for bipedal walking due to the real impulse force caused by the differences of dynamics properties and ground condition between the demonstrator and the imitator.

According to the principle of angular impulse and momentum about *O* in the imitator, the following two equations can be obtained.

$$I_O(w_B)_1 + r \times \int P dt = I_O w, \tag{9}$$

$$I_O w + r \times \int R dt = I_O(w_B)_2, \tag{10}$$

where I_O is the moment of inertia of the body about *O* that moves toward the stationary body. The subscription, '*B*' denotes the moving body, and '1' and '2' mean the state before and after the collision, respectively. Then, the coefficient of restitution, *e*, is given as

$$e = \frac{\int R dt}{\int P dt}. \tag{11}$$

Substituting Eq. (9) into Eq. (11) after eliminating the angular velocity *w* from Eqs. (9) and (10) yields

$$d(\frac{1+e}{e})\int R dt = I_O(w_B)_2 - I_O(w_B)_1 \tag{12}$$

Taking into account of a very short period of time from the time just before the collision to the time just after the impact, we may rewrite Eq. (12) as

$$d(\frac{1+e}{e})R = I_O \frac{d}{dt} w_B \approx \dot{H}_O \quad (13)$$

It is now straightforward to rewrite Eq. (13) as

$$d(\frac{1+e}{e})R = \dot{H}_G + r_G \times \dot{L} \quad (14)$$

Finally, the unknown reactive impulse force of the imitator is given by

$$R = \frac{e}{d(1+e)}(\dot{H}_G + r_G \times \dot{L}) \quad (15)$$

Since the direction of the landing foot is kept identical between the demonstrator and the imitator, the distance, *d*, between a fixed point *O* and the landing leg, or the stride interval, of the imitator can be determined. However, the angular momentum may not be conserved in the imitator owing to the transient interaction of the foot with the ground as mentioned above. If we take a careful look at Eq. (15), *d* is only a variable that is controllable, yet affects the magnitude of the unknown impulse force. Here the unknown impulse force of the imitator should be controlled such that the stability requirement of the imitator can be satisfied. Therefore, if *d* of the imitator is adjusted by controlling the position of the COM of the imitator, the imitator is expected to be ready to walk as stably as possible. More details are given in Section III.

C. Kinematics and dynamics adaptation

This subsection explains how the perceived data can be accommodated through the SAA. (See Fig. 4.)

(1) Phase I: A motion capture system records the trajectories of the link in interaction with the environment and the trajectories of the estimated COM of the demonstrator.

(2) Phase II: The captured trajectories are fed to the SAA. Under the condition that the direction of the link interacting with the ground should be kept as identical as possible, the joint angle trajectories of the imitator are generated. Here, care should be taken not to exceed the

maximum torque of the imitator that also affects the locomotion stability. To cope with this problem, the waist position of the imitator is optimized in the following section.

(3) Phase III: The imitator joint angle trajectories can be controlled by a neural oscillator network. This process will compensate for the discrepancy of the dynamic properties between the demonstrator and the imitator [18-19], [24].

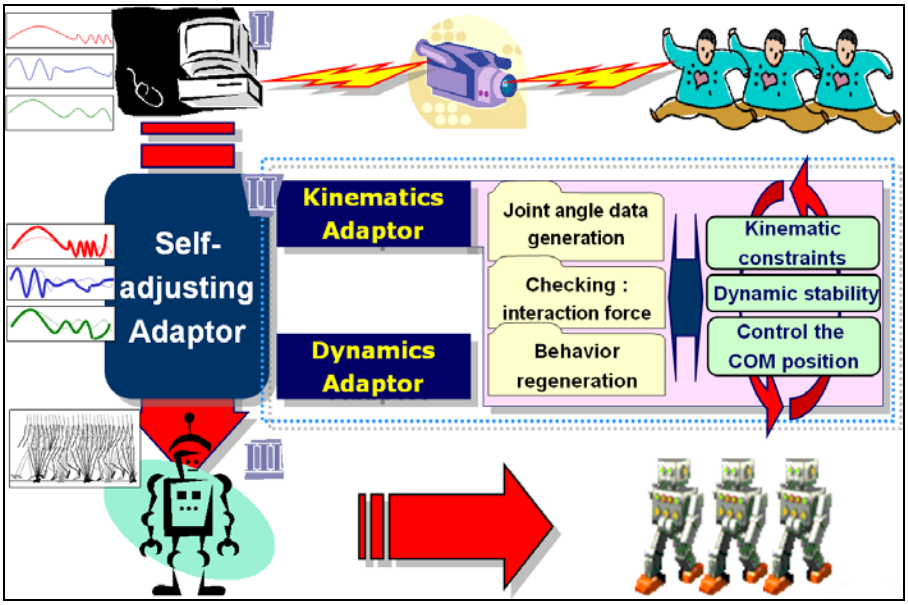

Fig. 4 Framework for imitation learning through self-adjusting adaptor

III. Application to Bipedal Locomotion

In this section, the proposed imitation method is applied to humanoid locomotion imitation illustrated in Fig. 5 (a). Fig. 5 (b) illustrates the kinematic schematic of the humanoid robot employed in this work. In the figure, RLEG-JOINT and LLEG-JOINT indicate right and left legs, respectively. RLEG-JOINT(0) and LLEG-JOINT(13) are engaged in the yawing motion. RLEG-JOINT(1), (5) and LLEG-JOINT(14), (18) are engaged in the rolling motion. RLEG-JOINT(2), (3), (4) and LLEG-JOINT(15), (16), (17) are engaged in the pitching motion, respectively. Because these notations are somewhat complex, we use different notations to easily explain the algorithm as shown in Fig. 5 (a).

In human gait, the single support (stance) phase consists of such three states as the heel contact (heel on), the sole contact, and the toe strike (heel off). The proposed approach only imitates the

sole contact that can be recognized from the sluggish area in the demonstrator's ankle joint trajectory. Based on this trajectory, the appropriate landing motion and lifting motion can be generated for the imitator. During the contact, the direction of the lower leg (or the ankle joint) is kept identical between the demonstrator and the imitator. Hence, the hip (or COM) trajectory of the imitator can be generated in the single support phase. If the COM trajectory does not satisfy the ZMP criterion, the position of the COM is adjusted in the sagittal plane through the optimization process to realize the pitching motion stably. Similarly, since the phases of the pitching and rolling motions should be coincident to maintain dynamic stability during locomotion, the COM position can be generated in the frontal plane through the optimization process within the period of the rolling motion. In practice, we can generate a possible rolling motion exploiting the reaction force direction and magnitude acquired from the foot force sensor, since the direction of the reaction force passes through the COM.

At the instance of foot contact with the ground, the height of the COM of imitator is scaled by a ratio of heights between the imitator and the demonstrator that becomes the same as the demonstrator's height of the COM. At this moment, the imitator can find its lower leg angle trajectories for the supporting leg to keep the lower leg direction identical with the demonstrator. Then, the ratio of the size of the foot trajectory of the imitator can be determined reflecting the difference between the position on the ground onto which the COM is projected and the position of the foot in the demonstrator and the imitator. Thus, the imitator's foot trajectory can be generated. Note that this trajectory is obtained solely by a kinematic viewpoint. The imitator now learned about the shape of the foot trajectory, the position of the COM, and the direction of lower leg to imitate as closely as possible the demonstrator's locomotion [19].

The underlying assumption behind this idea is that the locomotion of the demonstrator should have been optimized to achieve stability, keeping the angular momentum constant about the COM of the body. This means that the direction of the ground reaction or the resultant force acting on the foot passes through the COM of the body. Thus, the imitator should keep the direction of lower leg in contact with the ground as well as the position of the COM identical with the demonstrator. This will enable the imitator to maintain stability to a large extent, if the imitator is kinematically and dynamically similar to the demonstrator. Note that the locomotion

trajectories can be optimized by changing the position of the COM to satisfy the ZMP criterion. Details are given by the following steps:

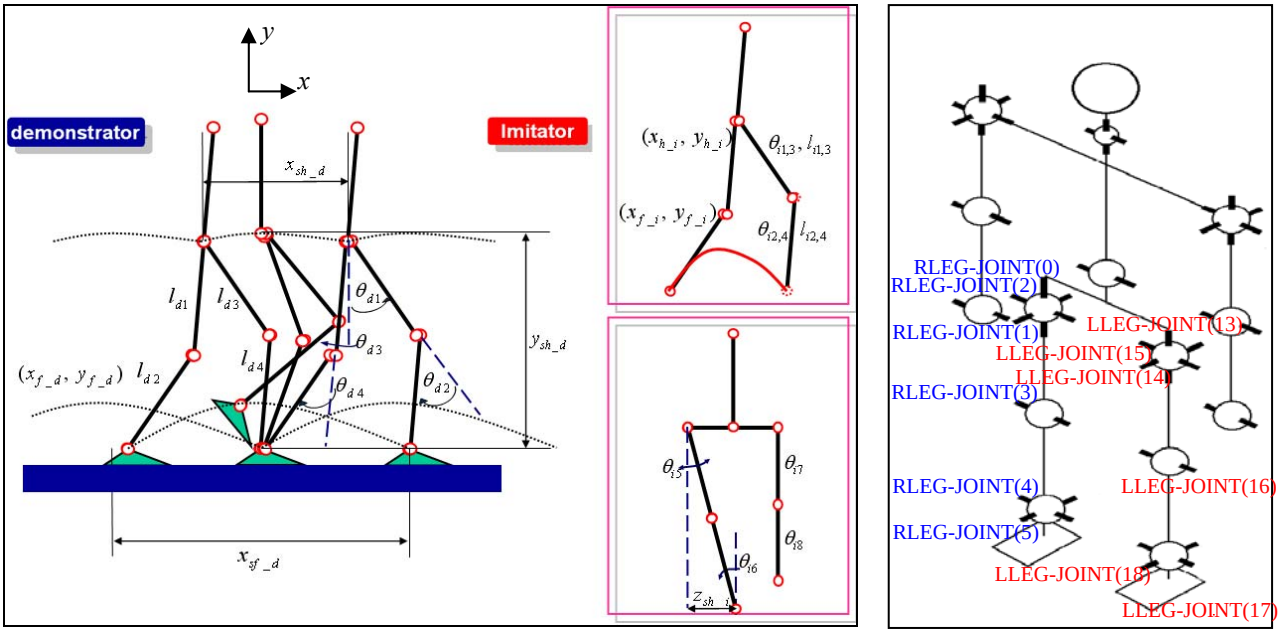

(a) (b)

Fig. 5 (a) Trajectories of biped locomotion, (b) Kinematic schematic of humanoid robot

x_{h_d}, y_{h_d}, x_{f_d}, y_{f_d}, and z_{h_d} are hip (or waist) and foot (or ankle) trajectories of the demonstrator in Cartesian coordinates acquired using a motion capture system. x_{sh_d}, y_{sh_d}, x_{sf_d}, y_{sf_d} and z_{sh_d} are the one stride interval of hip and foot of the demonstrator, respectively. l_{d1} and l_{d2} indicate the lengths of the upper and lower limb of the swing leg of the demonstrator as seen in Fig. 5. l_{d3} and l_{d4} are the lengths of the supporting leg in the figure. Note that the subscription, '*d*', in those lengths denotes the demonstrator and the subscript '*i*' is used for the imitator in the figure and the entire paper. Thus, θ_{i1} and θ_{i2} are the joint angles of the upper and lower limb of the swing leg of the imitator, respectively. θ_{i3} and θ_{i4} are the joint angles of the supporting leg of the imitator. The locomotion trajectories are switched between the two legs consecutively in the entire period of locomotion.

(1) Step 1: Obtain the trajectories of the hip and the foot of demonstrator in Cartesian coordinates from the motion capturing process: x_{h_d}, y_{h_d}, x_{f_d}, y_{f_d}, and z_{h_d} are given.

(2) Step 2: Determine the joint angle data for the demonstrator by solving the inverse kinematics problem. In the sagittal plane, θ_{d1}, θ_{d2}, θ_{d3}, and θ_{d4} are calculated as follows:

$$\theta_{d1,3} = \pi/2 + \tan^{-1}(y_{f,h\_d} / x_{f,h\_d}) - \tan^{-1}(\alpha/(k + l_{d1,3}^2 - l_{d2,4}^2),$$
$$\theta_{d2,4} = \tan^{-1}(\alpha/(k - l_{d1,3}^2 - l_{d2,4}^2)), \quad (16)$$

where $\alpha = \sqrt{((k + l_{d1,3}^2 + l_{d2,4}^2)^2 - 2(k^2 + l_{d1,3}^4 + l_{d2,4}^4)}$, $k = x_{f,h\_d}^2 + y_{f,h\_d}^2$

In the same manner, θ_{d5} and θ_{d6} can be obtained by Eq. (16) replacing x_{f,h_d} with z_{h_d}. Note that the first row in Eq. (16) contains two equations for θ_{d1} and θ_{d3} such that the first element of the subscript of every variable on the right-hand side of the equation corresponds to θ_{d1} and the second element θ_{d3}. The same notation is applied to entire equations.

(3) Step 3: Scale down (or up) the link length of demonstrator so that demonstrator and imitator have identical overall height and regenerate foot and hip trajectories: x'_{h_d}, y'_{h_d}, x'_{f_d}, y'_{f_d}, and z'_{h_d}

$$\begin{aligned}
y'_{f_d} &= l_{d1}\rho_f \cos\theta_{d1} + l_{d2}\rho_f \cos(\theta_{d1} + \theta_{d2}),\\
x'_{f_d} &= l_{d1}\rho_f \sin\theta_{d1} + l_{d2}\rho_f \sin(\theta_{d1} + \theta_{d2}),\\
y'_{h_d} &= l_{d3}\rho_h \cos\theta_{d3} + l_{d4}\rho_h \cos(\theta_{d3} + \theta_{d4}),\\
z'_{h_d} &= l_{d3}\rho_h \sin\theta_{d3} + l_{d4}\rho_h \sin(\theta_{d3} + \theta_{d4}),\\
x'_{h_d} &= l_{d3}\rho_h \sin\theta_{d3} + l_{d4}\rho_h \sin(\theta_{d3} + \theta_{d4})
\end{aligned} \quad (17)$$

where $\rho_f = \dfrac{l_{i1} + l_{i2}}{l_{d1} + l_{d2}}$, $\rho_h = \dfrac{l_{i3} + l_{i4}}{l_{d3} + l_{d4}}$

(4) Step 4: Keep the direction of lower leg under contact status to yield a posture of the intended goal. Then, the joint angles of imitator can be obtained as follows:

$$\theta_{i1,3} = \cos^{-1}\{\frac{l_{d1,3}\rho_{f,h}\cos\theta_{d1,3} + (l_{d2,4}\rho_{f,h} - l_{i2,4})\cos(\theta_{d1,3} + \theta_{d2,4})}{l_{i1,3}}\} \quad (18)$$

$$\theta_{i2,4} = (\theta_{d1,3} + \theta_{d2,4}) - \theta_{i1,3}, \quad (19)$$

where $\rho_{f,h} = (l_{i1,3} + l_{i2,4})/(l_{d1,3} + l_{d2,4})$ and ($\theta_{d1,3}$+$\theta_{d2,4}$) mean the direction of lower leg of the demonstrator. This procedure is performed when the demonstrator's foot is fully in contact with

the ground.

(5) Step 5: Generate foot and hip trajectories of imitator, multiplying the constant of ratios defined below to the scaled trajectories of foot and hip of demonstrator obtained from *Step 3* as

$$y_{f\_i} = ratio_{y\_f} y'_{f\_d},\ x_{f\_i} = ratio_{x\_f} x'_{f\_d},\ y_{h\_i} = ratio_{y\_h} y'_{h\_d}$$
$$x_{h\_i} = ratio_{x\_h} x'_{h\_d},\ z_{h\_i} = ratio_{z\_h} z'_{h\_d}, \tag{20}$$

where $ratio_{x\_f,h} = \left|1 - \frac{x_{f,h\_i}}{x_{f,h\_d}}\right|$, $ratio_{y\_f,h} = \left|1 - \frac{y_{f,h\_i}}{y_{f,h\_d}}\right|$, $ratio_{z\_h} = \left|1 - \frac{y_{h\_i}}{y_{h\_d}}\right|$

$$x_{f,h\_i} = l_{d1,3}\rho_{f,h}\sin\theta_{d1,3} + l_{d2,4}\rho_{f,h}\sin(\theta_{d1,3} + \theta_{d2,4}) - (l_{i1,3}\sin\theta_{i1,3} + l_{i2,4}\sin(\theta_{i1,3} + \theta_{i2,4}))$$
$$y_{f,h\_i} = l_{d1,3}\rho_{f,h}\cos\theta_{d1,3} + l_{d2,4}\rho_{f,h}\cos(\theta_{d1,3} + \theta_{d2,4}) - (l_{i1,3}\cos\theta_{i1,3} + l_{i2,4}\cos(\theta_{i1,3} + \theta_{i2,4}))$$
$$z_{h\_i} = l_{d3}\rho_h\sin\theta_{d3} + l_{d4}\rho_h\sin(\theta_{d3} + \theta_{d4}) - (l_{i3}\sin\theta_{i3} + l_{i4}\sin(\theta_{i3} + \theta_{i4}))$$

(6) Step 6: Finally, acquire the joint angle of imitator by inverse kinematics, which is basically the same as Eq. (16), and judge whether the obtained values are reasonable or not in kinematic and dynamic sense: θ_{i1}, θ_{i2}, θ_{i3}, θ_{i4}, θ_{i5}, and θ_{i6}

(7) Step 7: If the kinematics constraint or stability problem arises, perform the optimization process to control the hip position of imitator as follows. During the optimization process (see Fig. 6), the imitator hip position is rearranged satisfying the following constraints. At first, the right foot and left foot should be in contact with the ground in the double support phase. At the same time, in the rearranged hip position, the regenerated locomotion trajectory should satisfy the ZMP criterion. These problems are formulated separately in the sagittal and frontal planes. Specifically, in the sagittal plane, the minimal adjusting amount of the hip trajectories is determined satisfying the above constraints. This minimization problem can be given as follows,

$$\min_{\Delta\theta_{i1}} f(\Delta\theta_{i1}) = \left| y_{f\_i}(\theta_{i1} + \Delta\theta_{i1}) - y'_{d\_i} \right|_y \tag{21}$$

subject to

$$i)\ y_R(\theta_{i1} + \Delta\theta_{i1}) = 0,\ y_L(\theta_{i1} + \Delta\theta_{i1}) = 0 \tag{22}$$

$$ii)\ \varepsilon_x \le x_{zmp}(\theta_{i1} + \Delta\theta_{i1}) \le \delta_x, \tag{23}$$

where y_R and y_L are the distance between the ground and the foot position at the right leg and left leg, respectively. A given ε_x and δ_x are the ZMP limitation of imitator's foot in the x direction. And

$$x_{zmp} = \frac{\sum_n m_n(\ddot{y}_n + g)x_n - \sum_n m_n \ddot{x}_n y_n - \sum_n I_{nz}\ddot{\theta}_{iz}}{\sum_n m_n(\ddot{y}_n + g)}, \; z_{zmp} = \frac{\sum_n m_n(\ddot{y}_n + g)z_n - \sum_n m_n \ddot{z}_n y_n - \sum_n I_{ix}\ddot{\theta}_{ix}}{\sum_n m_n(\ddot{z}_n + g)}, \tag{24}$$

where $y_n = l_n \cos\theta_n$, $x_n = l_n \sin\theta_n$, $z_n = l_n \sin\theta_n$ for $n = 1 \sim 6$

Similarly, the minimization problem in the frontal plane can be formulated as

$$\min_{\Delta\theta_{i5}} f(\Delta\theta_{i5}) = \left| z_{h\_i}(\theta_{i5} + \Delta\theta_{i5}) - z'_{h\_d} \right|_z \tag{25}$$

subject to

$$i) \; z_L(\theta_{i5} + \Delta\theta_{i5}) = 0 \tag{26}$$

$$ii) \; \varepsilon_z \le z_{zmp}(\theta_{i5} + \Delta\theta_{i5}) \le \delta_z, \tag{27}$$

where z_L is the distance between the maximum displacement of the COM in the desired and modified trajectories. ε_z and δ_z are the ZMP limitation of imitator's foot in the z direction. The above optimization process can be performed at each time interval, $t=kT$ for $k=1\sim n$, in the entire period of locomotion. T denotes one stride interval. This enables the imitator to acquire the upper leg angle trajectories offering a dynamically stable COM height. The COM position is controlled by $\Delta\theta_{i1}$ on which θ_{i2}, θ_{i3}, and θ_{i4} are dependent. Also, θ_{i6} is dependent on $\Delta\theta_{i5}$. Therefore, if the imitator's foot and hip trajectories are obtained, which are the best possible trajectories within stability limits, the required joint angles of each leg for the imitator can be calculated by solving the inverse kinematics problem as mentioned in *Step 2*. In some cases, the allowable limits of the actuator need to be rigorously analyzed.

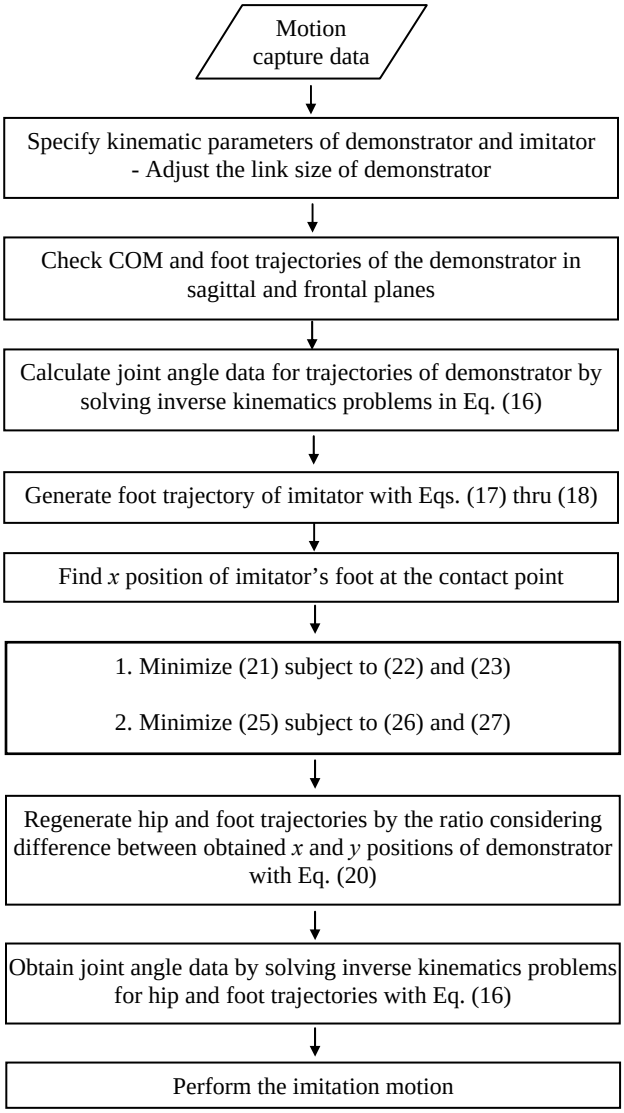

Fig. 6 Flowchart of SAA for imitator pattern generation

IV. Simulation Results and Discussion

We performed simulations to verify the validities of the SAA using OpenHRP. A built-in test model in OpenHRP is employed as the demonstrator. The same model with variable link lengths and an off-the-shelf humanoid robot are employed as the imitator as listed in Table 1. The demonstrator and imitators in Cases 1 through 4 have the same total leg length that is the sum of the lengths of upper and lower leg. However those models have different length ratios between the upper and lower leg. The imitators in Cases 5 through 9 have different total length. In particular, Case 9 model shows differences in the number of degrees of freedom, the kinematic structures, and the dynamic properties including the COM position, the mass and moment of

inertia for each link, and the torque limit at each joint. Fig. 7 is a reference motion data obtained by virtually capturing the locomotion trajectories of the demonstrator. The upper and lower lines are the *x*- and *y*-trajectories of one gait cycle in time, respectively, in Cartesian coordinates. They represent the foot and hip trajectories of the demonstrator in swing phase of the left and right leg in turn. Figs. 8 and 9 are the joint angle data of the demonstrator legs obtained by solving the inverse kinematics problem given the foot and hip trajectories as shown in Fig. 7.

Table 1 shows the height and limb length difference between various imitator models with respect to the demonstrator. We pay attention to the kinematics constraints that can be violated either when the leg joint angles satisfying Eqs. (22) and (26) at the moment of heel strike might not exist, or when the leg joint trajectories of one stride (connecting heel strike to heel strike) might not exist. These problems mainly occur when the length of the imitator's upper leg is shorter than the demonstrator's upper leg, that is, the generated area of the foot trajectory geometry for the imitator is larger than that for the demonstrator. To overcome these difficulties, we modified the height of the COM of the imitator through the optimization process that gave the minimum value needed to satisfy the ZMP criterion. For Cases 3, 5, 7 and 9, the height of the COM was modified, while there were no violations on the kinematics constraints for Cases 1, 2, 4, 6 and 8. All calculated joint torques were within the allowable limit in all cases of Table 1.

Table 1. Specifications of Employed Models

	Total Height	**Case No.**	**Upper Leg[m]**	**Lower Leg[m]**	**Kinematic structure**	**Dynamic property**
Imitator	Same	1	0.3435	0.31	Same	Same
		2	0.3635	0.29	Same	Same
	Same	3	0.3035	0.25	Same	Same
		4	0.4035	0.35	Same	Same
	0.8times	5	0.2728	0.25	Same	Same
		6	0.2928	0.23	Same	Same
	1.2times	7	0.4142	0.37	Same	Same
		8	0.4342	0.35	Same	Same
Imitator HOAP-1	Different	9	0.1	0.1	Different	Different
Demonstrator			**0.3535**	**0.3**		

There are significant dissimilarities in the limb length ratio in Cases 3 and 8, and differences in dynamic properties and kinematic structure in Case 9. Figs. 10 and 11 are the hip and knee

joint angle trajectories of the imitator. In these figures, the middle black line is obtained using Eq. (19) through the SAA, and the red dashed line is the original demonstrator data drawn by Eq. (19). The accordance of the two graphs at both ends (encircled with black dotted lines) implies that the direction of the lower leg of the demonstrator and the imitator is kept identical at the moment of heel strike. It can be verified that the foot trajectory of the imitator is similar to that of the demonstrator. As expected, the stride interval of the imitator is longer than that of the demonstrator in Cases 3 and 9. To prevent the imitator from violating the kinematic constraints, the imitator's COM height needs to be modified. In contrast, we can observe that the original joint angle trajectories of the demonstrator are inadmissible for the imitators, since it causes abnormally large ground reaction forces and tilted trajectory as shown in Fig. 12. Also, Figs. 19 and 26 in Case 8 and 9 show similar inadmissible trajectories.

Now we simulate the biped locomotion on the software platform OpenHRP [20] employing the PD and HighGain controllers. For the individual cases, one model is actuated by the original captured data and the other model is actuated by the data modified by the SAA. In Case 7 that the length of upper leg of imitator is shorter than that of demonstrator, Figs. 13 and 14 represent the ankle joint's relative force, relative torque, and actuating torque of the imitator when the SAA is not incorporated and incorporated, respectively. It is evident that the locomotion becomes unfeasible in the white dashed line area in Fig. 13, while the rhythmic patterns are maintained in Fig. 14. Similar results are also observed in Figs. 20 and 21. Specifically, Figs. 13, 14, 20 and 21 present the ankle joint of left leg, LLEG-JOINT(17) in Fig. 5 (b). In the simulation results, the first 4s show the initial motion to get into the starting posture. During this period, the motions are considered stable due to the dynamic similarity between the imitator and the demonstrator. However, the difference is evident between whether the SAA is incorporated or not from the very first (half) stride made by the right leg. In case that the original demonstrator data is employed, as shown in Figs. 13 and 20, although the stability is somehow maintained in the first step, the ground reaction force becomes very significant from the second step and the stability is lost at the fourth step. Figs. 15 and 16 are the snapshots of OpenHRP animation. The imitator actuated by the original captured data falls down and the same imitator actuated by the modified data with the SAA walk stably. In Case 8, the length of upper leg of imitator is longer than that of demonstrator, and we can observe from Figs. 17 through 23 that the SAA makes the imitator

possible to imitate a demonstrator. The current simulations were performed for the imitators that have different link length from the demonstrator. If there exist dynamics dissimilarities as well, the imitator's motion becomes completely infeasible when the SAA is not incorporated.

Finally, the proposed locomotion by imitation scheme is applied to a real humanoid robot, HOAP-1 (Fujitsu Automation Ltd.,). After the sequence of overall steps in SAA is completed to obtain an appropriate data for HOAP-1 (see Figs. 24 to 26), it is verified on OpenHRP as shown in Figs. 27 and 28. The robot fails to maintain its stability with the original perceived data and falls down from the first stride as shown in Fig. 27. Figs. 28 and 29 show the good agreement between the simulation results and experimental verifications of imitated walking of the robot facilitated by the proposed method. In the experiment, a host computer is employed to implement the SAA module and send the accommodated data to the robot through universal serial bus interface every 1ms. Note that our SAA cannot completely compensate for the apparently different dynamics. Therefore, in the experiment, the position of the hip joint, the intersection point of the axes for RLEG-JOINT(0), (1) and (2) or LLEG-JOINT(13), (14) and (15), was changed slightly by 0.1cm backward from the estimated optimal position.

This paper so far discussed the kinematic adaptation process of the SAA. To realize a more functionally robust SAA, we need to consider an efficient way of dealing with the dynamic characteristics of the demonstrator and the imitator. In practice, it is required to estimate the mass distribution within the body segments, in addition to the length of the segments, of the demonstrator. Instead of tackling this problem directly, we have attempted to minimize the difference in body dynamics between the demonstrator and the imitator by changing the imitator's height of the COM reflecting the ZMP criterion. From the simulation results of Case 9, it was verified that the SAA compensated, to a large extent, for the differences of dynamics. Thus, we can obtain dynamically admissible trajectories for the imitator. Most of the remaining problems associated with unknown terrain as well as additional uncertainty in dynamic characteristics can be compensated by exploiting a neural oscillator network. The neural oscillator is known to be robust to changes in dynamics parameters or environment disturbances over a specific range of frequencies. This will be addressed in future phases of this work.

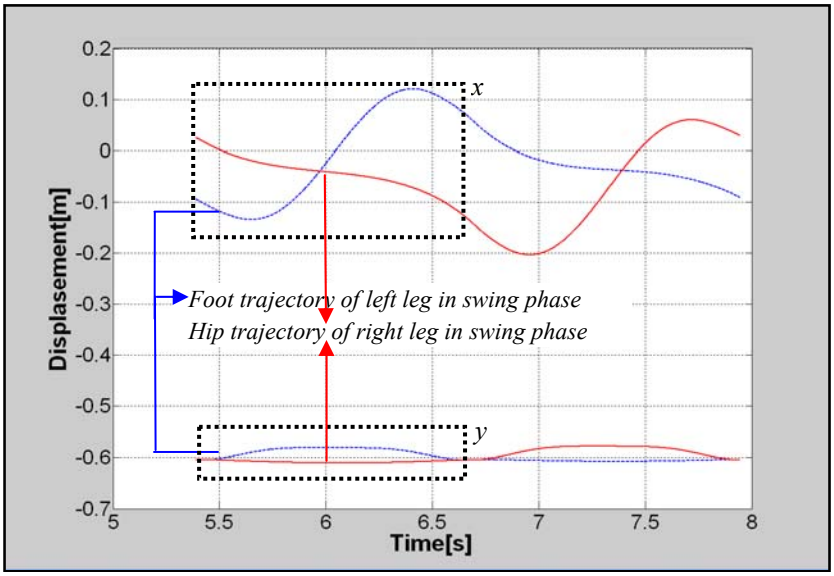

Fig. 7 Foot and hip trajectories of the demonstrator in x- and y-coordinates

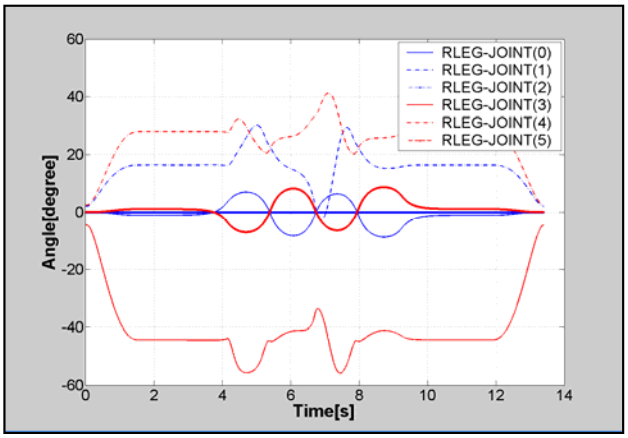

Fig. 8 Trajectories of right leg-joint angles of the demonstrator

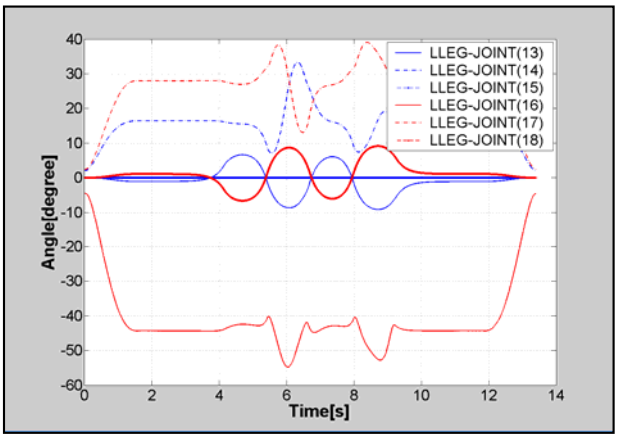

Fig. 9 Trajectories of left leg-joint angles of the demonstrator

A. Case 3

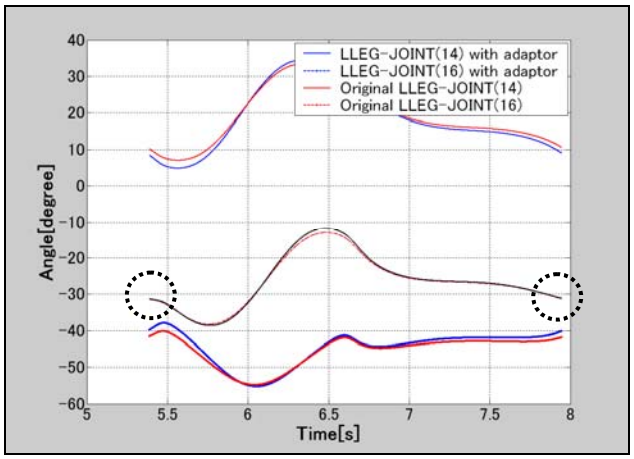

Fig. 10 Trajectories of left leg-joint angles of Demonstrator and imitator

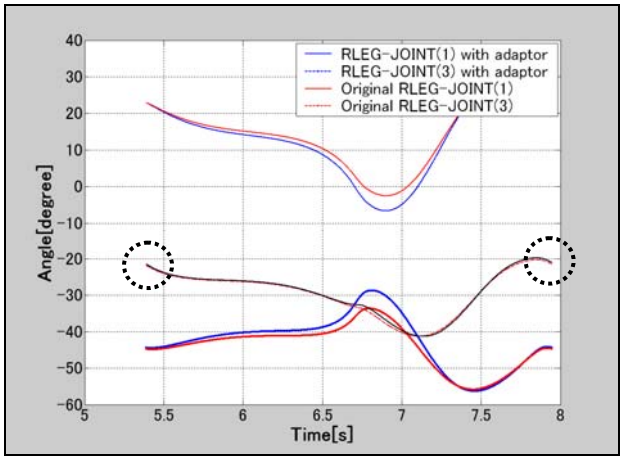

Fig. 11 Trajectories of right leg-joint angles of Demonstrator and imitator

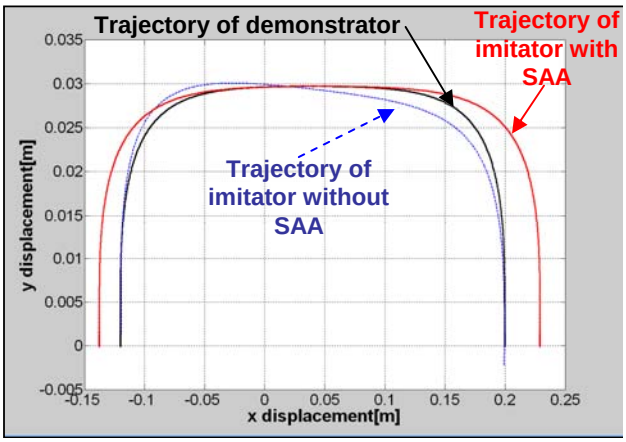

Fig. 12 Regenerated imitator foot trajectory

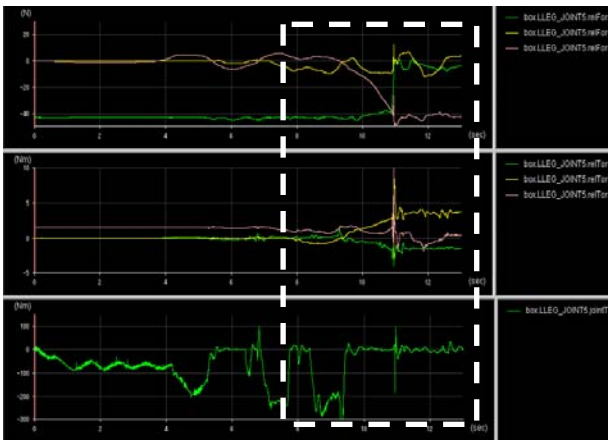

Fig. 13 Relative force, torque, and actuating torque at ankle joint without SAA

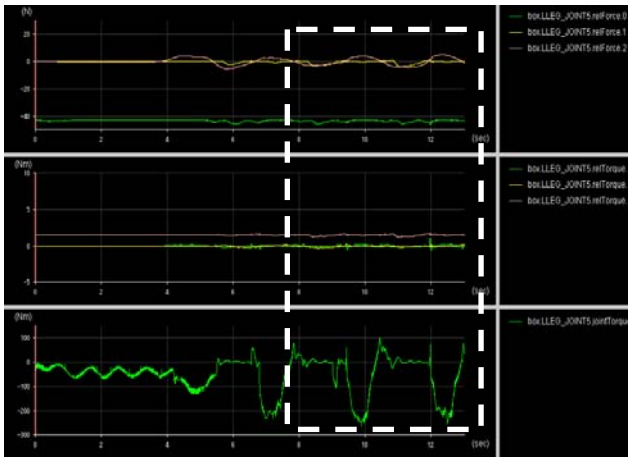

Fig. 14 Relative force, torque, and actuating torque at ankle joint with SAA

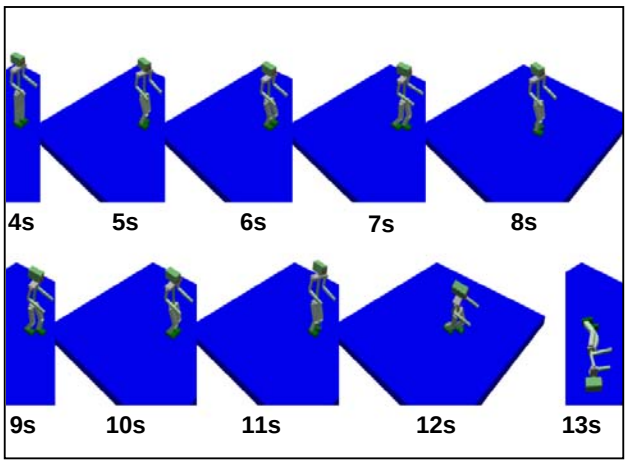

Fig. 15 Snapshots of imitator's locomotion without SAA

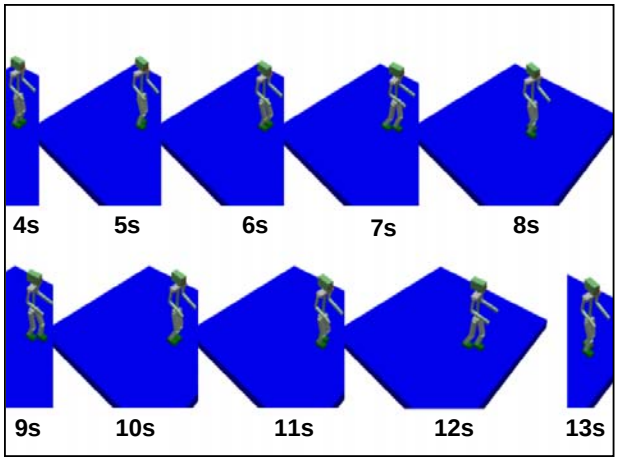

Fig. 16 Snapshots of imitator's locomotion with SAA

B. *Case 8*

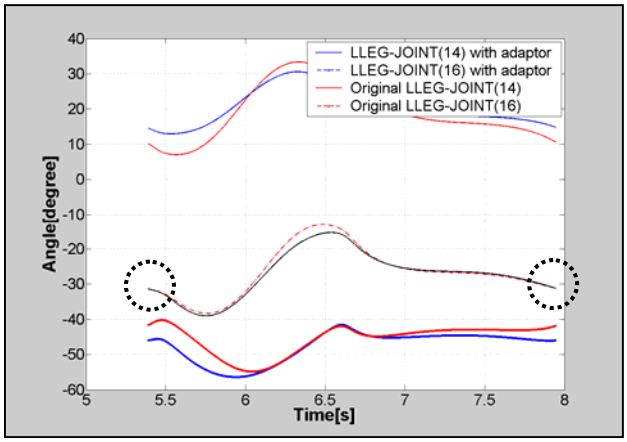

Fig. 17 Trajectories of left leg-joint angles of demonstrator and imitator

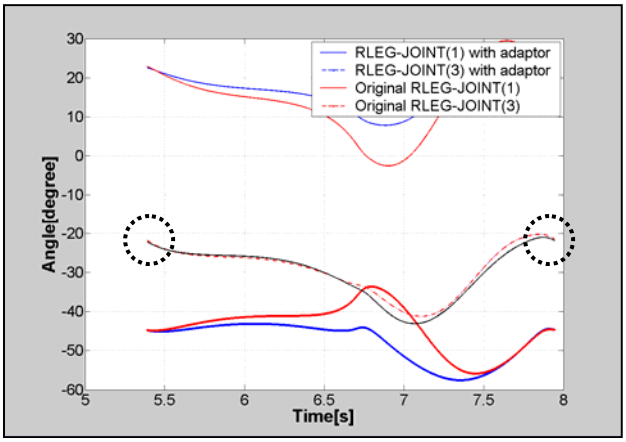

Fig. 18 Trajectories of right leg-joint angles of demonstrator and imitator

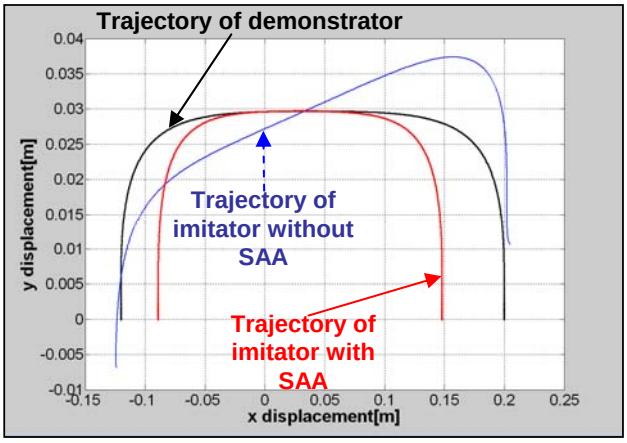

Fig. 19 Regenerated imitator foot trajectory

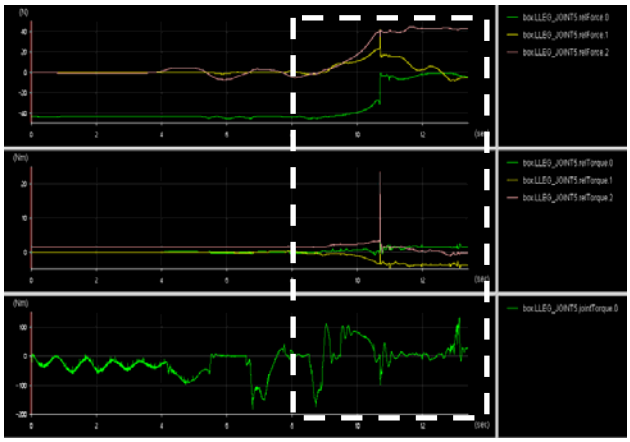

Fig. 20 Relative force, torque, and actuating torque at ankle joint without SAA

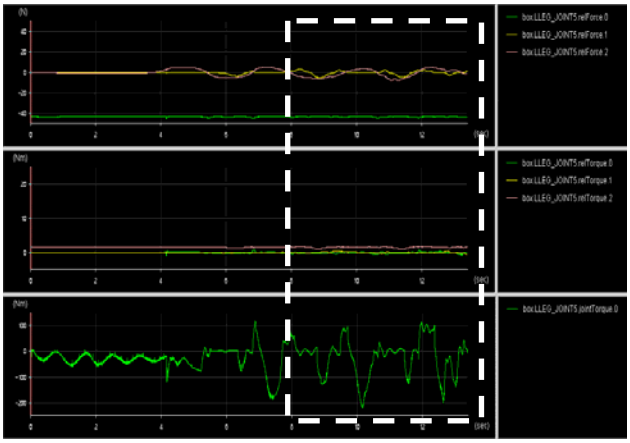

Fig. 21 Relative force, torque, and actuating torque at ankle joint with SAA

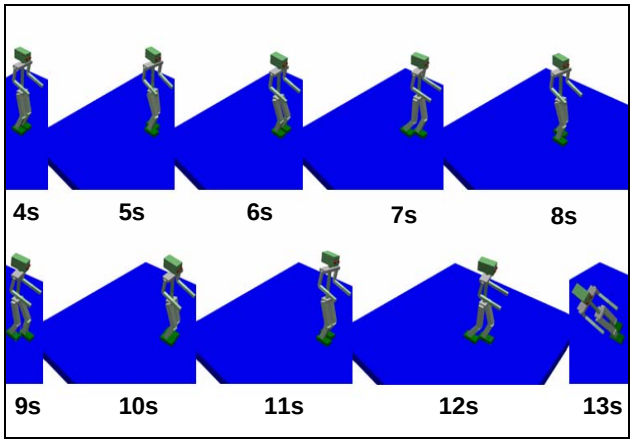

Fig. 22 Snapshots of imitator's locomotion without SAA

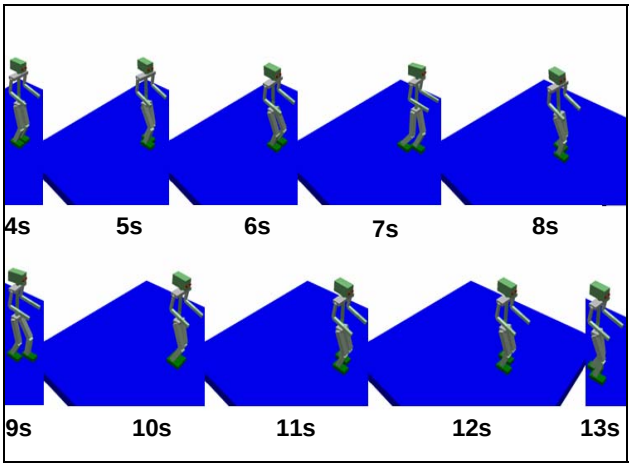

Fig. 23 Snapshots of imitator's locomotion with SAA

C. *Case 9*

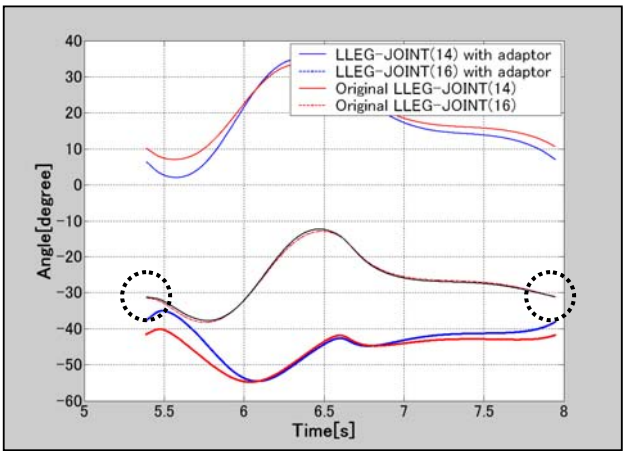

Fig. 24 Trajectories of left leg-joint angles of demonstrator and Hoap-1

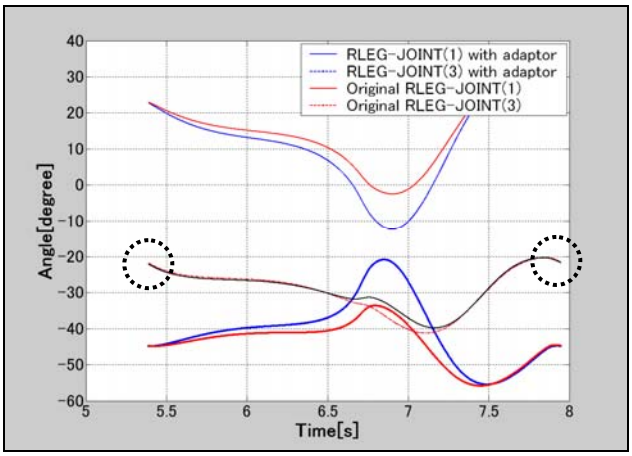

Fig. 25 Trajectories of right leg-joint angles of demonstrator and Hoap-1

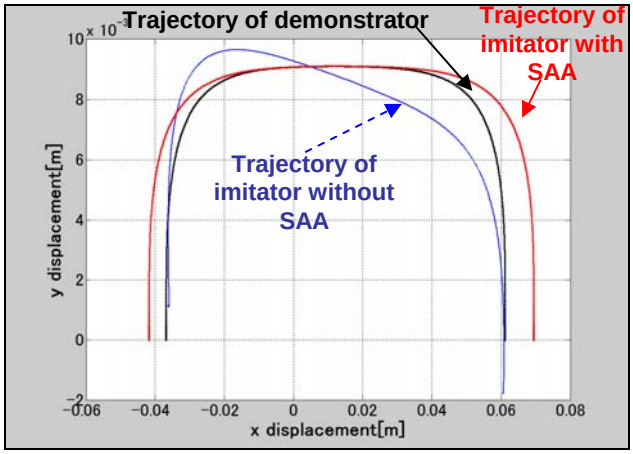

Fig. 26 Regenerated Hoap-1 foot trajectory

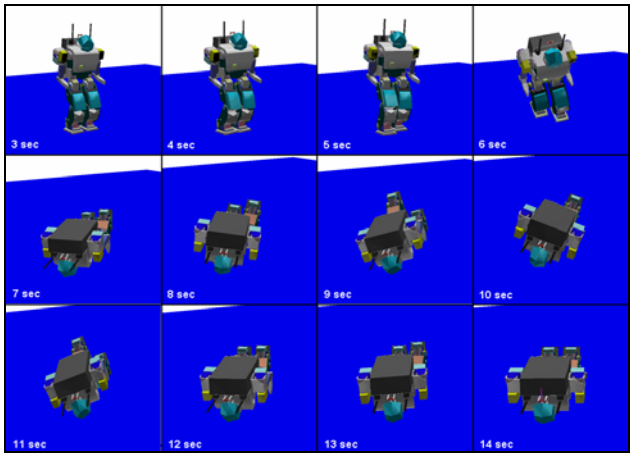

Fig. 27 Snapshots of imitator's locomotion without SAA

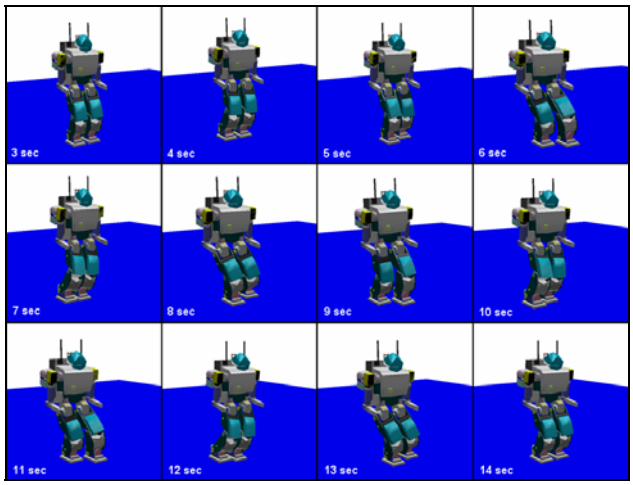

Fig. 28 Snapshots of imitator's locomotion with SAA

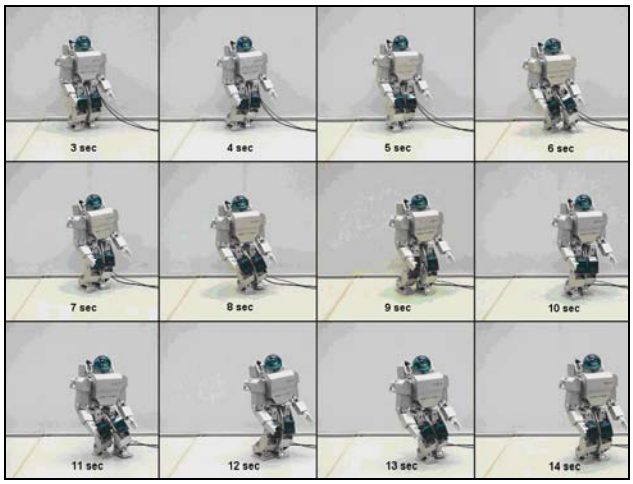

Fig. 29 Snapshots of locomotion of a real humanoid

V. Conclusion

Learning by imitation was investigated considering that there apparently exist significant interactions between the imitator and its environment. In particular, a new framework for imitation was presented to enable a humanoid robot to learn behaviors from other robots. No works clearly explained how imitation techniques could be incorporated into learning that guarantees the achievement of the intended goal of demonstration. This work led to the formulation and verification of a practical approach to the real-world learning by imitation. Our major contributions can be summarized as: 1) this work specifically investigated the case when the robot was closely interacted with the environment. 2) this approach allowed for learning from other robots in different shapes and bodies. 3) the imitation technique was simply performed by observing only the specific body points of the demonstrator and absorbing uncertainties associated with interactions between the robot and its environment. To implement these features, the self-adjusting adaptor was developed, which allows individual imitators to achieve the goal of the perceived motion. Specifically, in the case of locomotion learning, the proposed adaptor was verified by simulations on the virtual humanoid robot simulator OpenHRP. Using a reference locomotion pattern originally designed for the test model in OpenHRP, the proposed adaptor could generate different locomotion patterns accommodated to nine humanoid models. In addition, we verified this proposed adaptor through experiments with a real robot. Overall, so far, we have had encouraging results that the proposed adaptor was useful for humanoid locomotion, which can be extended to more sophisticated motion generation problems. Finally, we will

include a neural oscillator network in our potential future version of the adaptor which is expected to compensate for unknown dynamic properties and external disturbances more effectively.

References

[1] M. Vukobratovic and D. Juricic, "Contribution to the Synthesis of Biped Gait," IEEE Trans. Bio-Med. Eng., vol. BME-16, no.1, pp. 1-6, (1969).

[2] M. Vukobratovic, "How to Control Artificial Anthropomorphic Systems," IEEE Trans. Syst., Man, Cybern., vol. SMC-3, no.5, pp. 497-507, (1973).

[3] S. Kajita, O. Matsumoto, and M. Saigo, "Real-time 3D Walking Pattern Generation for a Biped Robot with Telescopic Legs," Proc. IEEE Int. Conf. on Robotics and Automation, pp. 2299-2306, (2001).

[4] J. Pratt, C.-M. Chew, A. Torres, P. Dilworth, and G. Pratt, "Virtual Model Control: An Intuitive Approach for Biped Locomotion," The Int. Journal of Robotics Research, vol. 20, no. 2, pp. 129-143, (2001).

[5] G. Endo, J. Nakanishi, J. Morimoto, and G. Cheng, "Experimental Studies of a Neural Oscillator for Biped Locomotion with QRIO," Proc. IEEE Int. Conf. on Robotics and Automation, pp. 598-604, (2005).

[6] C. Nehaniv and K. Dautenhahn, "Of Hummingbirds and Helicopters: An Algebraic Framework for Interdisciplinary Studies of Imitation and Its Applications," An Interdisciplinary Approaches to Robot Learning, J. Demiris and A. Birk (Eds.), World Scientific Publishing Co., pp. 136-161, (2000).

[7] A. Billard and R. Siegwart, "Robot Learning from Demonstration," Robotics and Autonomous Systems, vol. 47, pp. 65-67, (2004).

[8] J. Demiris and G. Hayes, "Do Robots Ape?," Proc. AAAI Fall Symp. on Socially Intelligent Agents, pp. 28-30, (1997).

[9] A. Dasgupta and Y. Nakamura, "Making Feasible Walking Motion of Humanoid Robots from Human Motion Capture Data," Proc. IEEE Int. Conf. on Robotics and Automation, pp. 1044-1049, (1999).

[10] T. Inamura, I. Toshima, H. Tanie, and Y. Nakamura, "Embodied Symbol Emergence Based on Mimesis Theory," The Int. Journal of Robotics Research, vol. 23, no. 4-5, pp. 363-377, (2004).

[11] A. J. Ijspeert, J. Nakanishi, and S. Schaal, "Movement Imitation with Nonlinear Dynamical Systems in Humanoid Robots," Proc. IEEE Int. Conf. on Robotics and Automation, pp. 1398-1403, (2002).

[12] S. Schaal, "Is Imitation Learning the Way to Humanoid Robots?," Trends in Cognitive Science, vol. 3, no. 6, pp. 233-242, (1999).

[13] K. Samejima, K. Katagiri, K. Doya, and M. Kawato, "Symbolization and Imitation Learning of Motion Sequence Using Competitive Modules," Trans. of the Institute of Electronics, Information, and Communication Engineers, vol. J85-D-II, no. 1, pp. 90-100, (2002).

[14] K. Samejima, K. Doya, and M. Kawato, "Inter-module Credit Assignment in Modular Reinforcement Learning," Neural Networks, vol. 16, no. 7, pp. 985-994, (2003).

[15] Y. Nakamura and M. Ghodoussi, "Dynamics Computation of Closed-Link Robot Mechanisms with Nonredundant and Redundant Actuators," IEEE Trans. on Robotics and Automation, vol. 5, no. 3, pp. 294-302, (1989).

[16] Y. Nakamura and K. Yamane, "Dynamics Computation of Structure-varying Kinematic Chains and Its Application to Human Figures," IEEE Trans. on Robotics and Automation, vol. 16, no. 2, pp. 124-134, (2000).

[17] K. Yamane and Y. Nakamura, "Dynamics Filter – Concept and Implementation of Online Motion Generator for Human Figures," IEEE Trans. on Robotics and Automation, vol. 19, no. 3, pp. 421-432, (2003).

[18] W. Yang and N. Y. Chong, "Goal-directed Imitation with Self-adjusting Adaptor Based on a Neural Oscillator Network," Proc. Int. Conf. on Advanced Robotics, pp. 404-410, (2005).

[19] W. Yang N. Y. Chong, C. Kim and B. J. You, "Locomotion Imitation of Humanoid Using Goal-directed Self-adjusting Adaptor," Proc. IEEE/RSJ Int. Conf. on Intelligent Robots and Systems, pp. 5650-5656, (2006).

[20] http://www.is.aist.go.jp/humanoid/openhrp/English/indexE.html

[21] C. A. A. Calderon and H. Hu, “Robot Imitation from Human Body Movements,” Proc. Int. Symp. on Imitation in Animals and Artifacts, pp. 1~9, (2005).
[22] M. J. Mataric, “Imitation in Animals and Artifacts,” Sensory-Motor Primitives as a Basis for Imitation: Linking Perception to Action and Biology to Robotics, pp. 392-422, The MIT Press, Cambridge, MA, (2002).
[23] M. J. Mataric and M. Pomplun, “Fixation Behavior in Observation and Imitation of Human Movement,” Cognitive Brain Research, Vol. 7, No. 2, pp. 191~202, (1998).
[24] W. Yang, N. Y. Chong, C. Kim and B. J. You, “Self-adapting Humanoid Locomotion Using a Neural Oscillator Network,” Proc. IEEE/RSJ Int. Conf. on Intelligent Robots and Systems, pp. 309-316, (2007).